Numerical analysis of TBM tunnelling in sand using a state parameter model

Conference Paper · September 2016

3 authors, including:

Bowen Yang
The University of Warwick
2 PUBLICATIONS **0** CITATIONS
SEE PROFILE

Benoit Jones
Inbye Engineering
10 PUBLICATIONS **13** CITATIONS
SEE PROFILE

Numerical analysis of TBM tunnelling in sand using a state parameter model

B.Yang[a]*, S.Utili[b], B.D. Jones[c]
[a] The University of Warwick, Coventry, UK
B.Yang.2@warwick.ac.uk
[b] The University of Warwick, Coventry, UK
s.utili@warwick.ac.uk
[c] The University of Cambridge, Cambridge, UK
bdj26@cam.ac.uk

Abstract

Although empirical and numerical methods of predicting ground movements due to tunnelling have had some success in clay soils, there remains considerable uncertainty about predictions in sand, because trough width is not constant but varies with volume loss, because constant volume behaviour cannot be assumed, and because of localisation. Based on numerical modelling of a centrifuge test using the Hardening Soil Model, a crucial feature of sand behaviour not been properly described in this model was identified – stress dilatancy. The state parameter sand model-Norsand catches the state dependent contraction and dilation behaviour of sand, and is capable of simulating the general behaviour of sand with a wide range of density. Therefore Norsand has for the first time been implemented in Plaxis3D in order to capture the stress dilatancy behaviour of sand. The formulas of the Norsand model for FEM software implementation are deduced. According to the literature, a user defined parameter is introduced into the original Norsand model: COMI for identification of the image point M_i. The Norsand model was found to give a better agreement with the measured settlement troughs at all values of volume loss. FEM simulation using Norsand will enable more accurate predictions of ground movements due to tunnelling in sand, providing better information about the risks to third party assets.

Keywords: *Tunnelling, TBM, Sand, NorSand, Soil mechanics, State parameter*

Introduction

Ground movement induced by TBM tunnelling in sand has been discussed a lot in the past years. The main cause of ground movement in TBM projects has been identified as the tunnel volume loss $V_{l,t}$ (Mair and Taylor 1997; Lee et al. 2004) induced by shield over-cutting and the dimensional difference between the shield and the lining. Rowe and Kack (1983) simplified the ground deformation mechanism induced by shield tunnelling as Figure 1a. The reason of the majority of the tunnel deformation is locating around the tunnel crown area is because as the shield advances, the weight of the lining will cause it to rest on the excavated tunnel invert. The similar phenomenon has been widely adopted by recent works (Pinto and Andrew J, 2000; Gonzalez and Sagaseta, 2001) (Figure 1b,c). Thus, this ground deformation pattern around tunnel is used in the present paper.

Having been studied for decades, numerical modelling becomes a useful tool for ground movement prediction especially when dealing with projects where complex underground structures and strata distributions are involved. The accuracy of the numerical modelling depends to large extent on the adequacy of the stress strain relationships that are used in the calculation (Azevedo 2002). The constitutive model adopted in the numerical modelling should be able to capture the key features of the stress paths and the soil behaviour in the projects. There are a large numbers of constitutive soil models in the literature, they are developed based on different concepts to address different geotechnical problems. Although, it is commonly agreed that the numerical prediction of the settlement troughs induced by tunnelling in sand is not easy. This is fundamentally due to the current soil models implemented in commercial numerical software are not developed specifically to capture the key features of soil behaviour during tunnelling in sand. For example, using the Hardening soil model (Schanz et al. 1999) which is suggested by the commercial numerical software Plaxis 3D in modelling sand behaviour, the key feature of sand - soil contraction/ dilation that significantly affects the ground deformation is poorly simulated (Figure 6). Furthermore, in an undrained soil, from surface to tunnel level, the soil volume loss $V_{l,s}$ almost stay consistent with the tunnel volume loss $V_{l,t}$ (Mair et al., 1993; Marshall et al., 2012) whereas for drained soils such as sands and gravels, shearing causes contraction and dilation which lead to an inconsistent $V_{l,s}$:$V_{l,t}$ ratio (Vorster et al., 2005; Marshall et al., 2012). The Norsand model developed by Jefferies (1993) based on the concept of state parameter (Been and Jefferies, 1985) and the infinity of normal consolidation line (NCL) (Ishihara et al. 1975) has been proved to be useful in simulating state dependent (relative density of soil sample) dilation and contraction (Jefferies and Been, 2006; Jefferies and Shuttle, 2005) of sand. Thus this model is selected for implementation in present work.

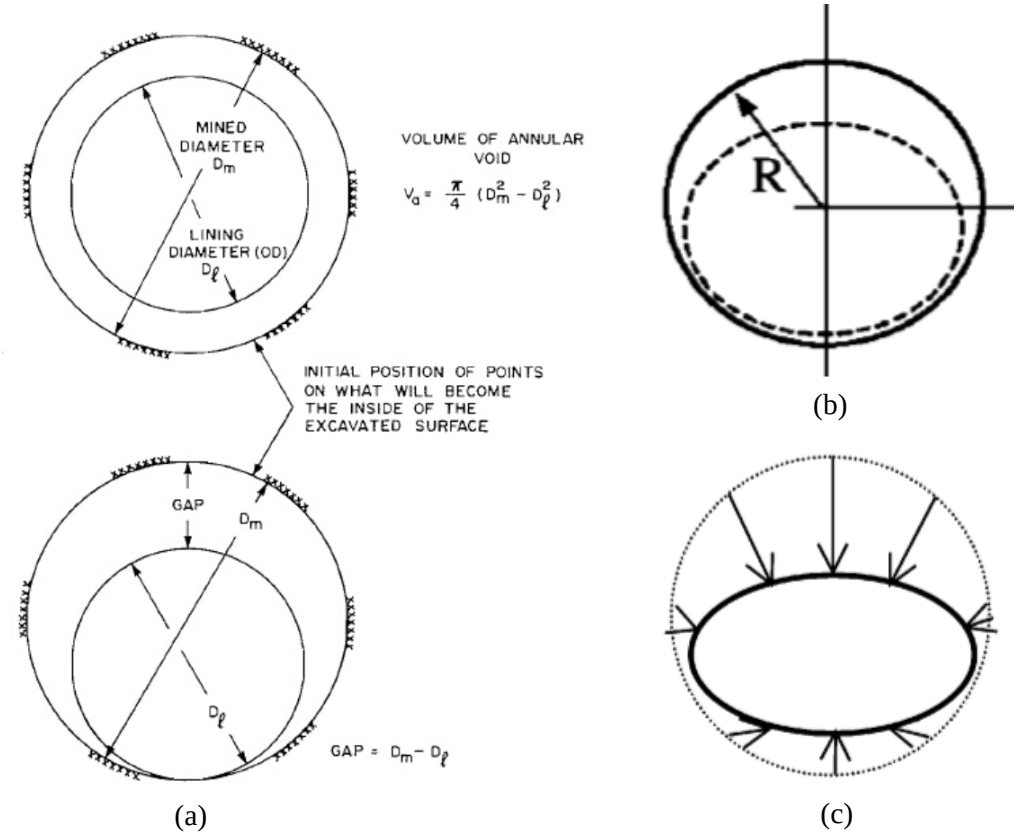

Figure 1. Patterns of ground deformations around tunnels. a). Rowe and Kack (1983); b). Pinto and Andrew J (2000); c). Gonzalez and Sagaseta (2001)

The case – Modelling a centrifuge model

Of particular relevance to this paper is the set of centrifuge tests performed by Marshall (2009). The size of the model tunnel is 62mm in diameter with its axis level at a depth of 180mm. With a centrifuge scaling factor N of 75, the centrifuge model represents a 4.65m diameter tunnel with its axis at a depth of 13.65m. The centrifuge test considers the particular situation in TBM tunnelling, as described in Figure 1, where the majority of the ground deformation occurs above the tunnel crown by using a fixed brass cylinder inside the latex tunnel model. In the centrifuge test, $V_{l,t}$ is controlled by extracting the fluid between the latex tunnel and the brass cylinder. In other words, the volume loss control procedure can be summarised as fix the inner tube and control the space between the two surfaces, then allow the latex deform freely. Ground deformation data is recorded from surface to tunnel crown level with $V_{l,t}$ = 0% to 5%. By modelling this green field condition centrifuge tunnel, variables such as ground water flow, structure-soil interaction and in-situ soil parameters other than soil behaviour itself are eliminated. As shown in Figure 2, the geometry and deformation pattern of the FEM model is consistent with the centrifuge model. The larger cylinder representing the latex membrane is free to move in all directions. The smaller cylinder of plate elements representing the brass cylinder is prescribed as zero deformation in all three directions.

The Soil model - Norsand

The equations of current Norsand model (Jefferies and Been, 2006) are selected to be implemented and to model the case, thus will be briefly discussed. As Schofield and Wroth (1968) mentioned, one kind of sand is a material that can exist in different states, the relative density is exactly a proper description of this state. The relative density can be defined as the difference between the current specific volume ν_0 and any desired reference specific volume. The principle of using relative density to predict the sand behaviour leads to the application of a state parameter. Many soil properties and sand behaviour are simple functions of the state parameter (Jefferies and Been, 2006). The state parameter ψ is defined as the difference between the current void ratio and the void ratio on CSL for current p level (Been and Jefferies, 1985).

$$\psi = \nu_0 - \nu_\Gamma \qquad [1]$$

By following Schofield and Wroth (1968), and to treat sands using the same constitutive constants at all densities, Jefferies (1993) developed the Norsand model which introduces the concept of infinity of the NCL (Ishihara et al. 1975). This model uses the image point pi (where the volumetric strain $\dot{\varepsilon}_p$ = 0) which is

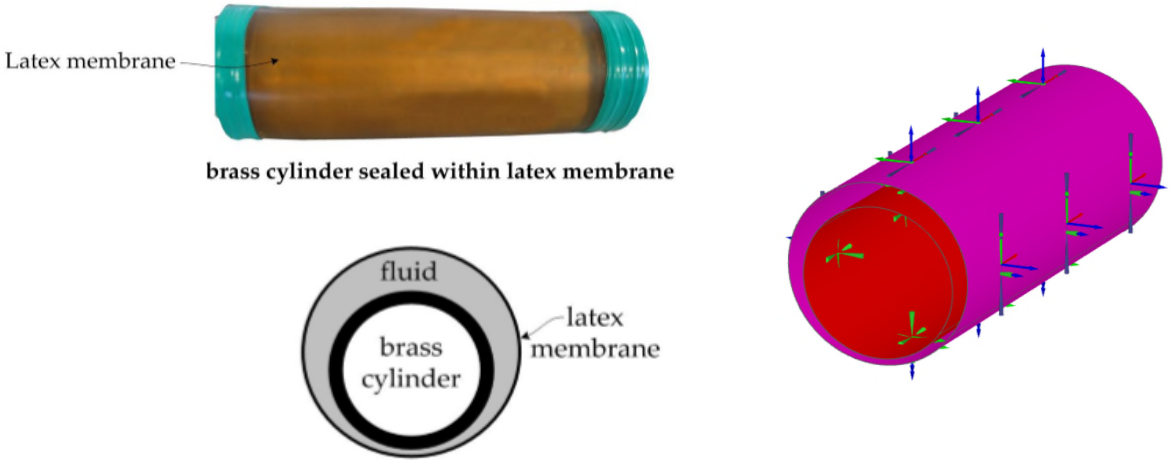

(a) (b)

Figure 2. The centrifuge (a) and FEM (b) tunnel models.

dependent on the state parameter ψ to describe the infinity of the NCL and control the shape and size of yield surface. The stress dilatancy rule used in Norsand is:

$$D^p = \mathrm{M_i} - \eta \qquad [2]$$

Where, D^p is the dilatancy ratio (plastic volumetric strain increment $\dot{\varepsilon}_p^p$ / plastic deviatoric strain increment $\dot{\varepsilon}_q^p$), ŋ is the stress ratio (mean stress p / deviatoric stress q), M_i is the stress ratio at the image point pi. The procedure of the development of the yield surface follows the conventional approach as Roscoe and Burland (1968) to derive the Cam Clay surface. The yield surface deduced from Eq. [2] is:

$$f(p, q, p_i) = M_i \left[1 - \ln\left(\frac{p}{p_i}\right)\right] - \eta \qquad [3]$$

An example of how the image point controls the hardening and softening of the yield surface is illustrated in Figure 3. Consider a sand sample that has been isotropically normally consolidated to point A, this situation gives the yield surface illustrated by surface a. Shear stress then applied, point B illustrates the yield surface hardens to surface b (where pi=p). During this stage of hardening, the volumetric strain is contractive due to normality. At the condition of pi=p, $\dot{\varepsilon}_p^p$=0, according to normality, the soil begin dilating during further hardening. The hardening does not stop until the minimum D^p is reached (the maximum off set of pi from p). The point where hardening switches to softening is denoted by surface c and point C. The soil dilation continues as long as the current mean stress p is on the left side of the image point, again, because of normality. When the surface is softened to surface d (b) where the image point and the CSL (Critical State Line where infinite shear occurs with $\dot{q}$ = 0) coincide at point D, the critical state is reached and the soil can deform without further softening/ hardening. In the Norsand model the determination of Mi is as follows (Jefferies and Shuttle 2002):

$$M_i = M\left(1 - |\psi_i| / M_{tc}\right) \qquad [4]$$

Where ψ_i refers to the state parameter at the image point, M_{tc} is a reference stress ratio that is deduced from the traxial compression test. Eq. [4] is an upper bond to the dense sand data. For completion, another two methods of deriving the value of M_i will be included in the present model:

$$M_i = M\exp(\mathrm{m}\psi) \ldots\ldots\ldots \mathrm{m} \approx 4 \qquad \text{(Li and Dafalias, 2000)} \qquad [5]$$

$$M_i = M + \mathrm{m}\psi \ldots\ldots\ldots \mathrm{m} \approx 4 \qquad \text{(Manzari and Dafalias, 1997)} \qquad [6]$$

Some latter developed bounding surface models (Li, 1997; Li et al., 1999; Li and Dafalias, 2000) tend to use more complex exponential dependence on ψ. Whichever ψ dependence is adopted, it should be always noticed that the stress dilatancy is ψ dependent. The choice of using Eq. [4], Eq. [5] and Eq. [6] is coded as an input parameter COMI in the present Plaxis 3D model. As illustrated in Figure 3, a limiting stress that terminates the hardening and softening is needed to act as an internal cap that marks the switch point between softening and hardening. This limiting stress is described as the form of a stress ratio:

$$\left(\frac{p_i}{p}\right)_{\max} = \exp\left(-\chi\psi_i / M_{tc}\right) \qquad [7]$$

where χ is a model property, Jefferies and Been (2006) concluded: under traxial compression condition, χ commonly lies between 2.5~4.5 and the value of χ does not vary greatly from one soil to another.

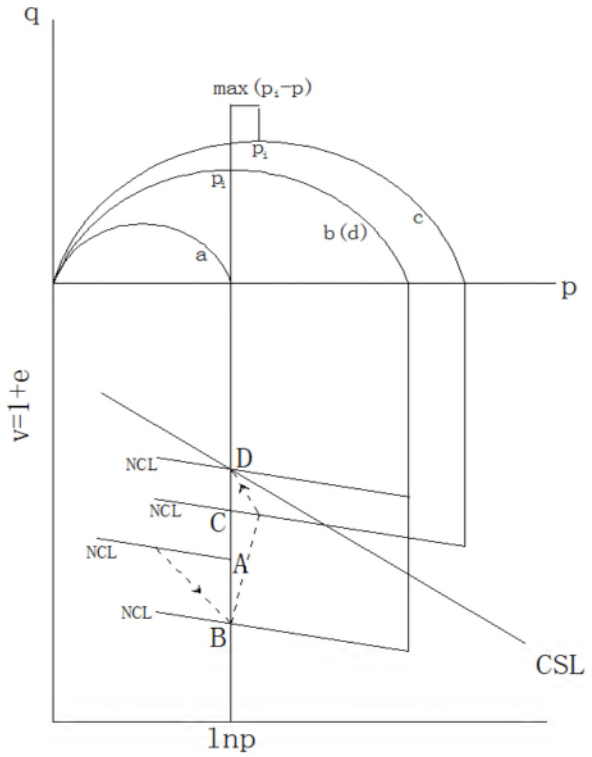

Figure 3. The infinity of NCL (v implies the specific volume; e is void ratio)

Numerical implementation

The above constitutive equations of the sand model are implemented into a finite element software Plaxis 3D as a user-defined subroutine. The user-defined subroutine in Plaxis calculation programme has been designed to have four main tasks: 1. Initialisation of state variables, where the calculated variables from last calculation step tells the position of the yield surface for current calculation step. 2. Calculation of effective stresses (use the matrix created in step 3 and 4). 3. Creation of effective stiffness matrix (not to be used unless yielding occurs). 4. Creation of elastic stiffness matrix. Thus, in the user defined subroutine, the problem becomes looking for the constitutive stresses according to the strain increments provided by Plaxis. The total strain increments include the elastic part and the plastic part, and is shown as:

$$\dot{\varepsilon}_{ij} = \dot{\varepsilon}_{ij}^{e} + \dot{\varepsilon}_{ij}^{p} \qquad [8]$$

where the superimposed dot denotes time derivative. As anisotropy is not included in present study, and for simplicity, we assume isotropic behaviour here, thus Norsand will be coded using the p – q plane. Then Eq. [8] becomes:

$$\dot{\varepsilon}_{v} = \dot{\varepsilon}_{v}^{e} + \dot{\varepsilon}_{v}^{p} \qquad [9]$$

$$\dot{\varepsilon}_{q} = \dot{\varepsilon}_{q}^{e} + \dot{\varepsilon}_{q}^{p} \qquad [10]$$

where the subscript v and q denotes volumetric and deviatoric strain respectively. For simplicity, the matrix used in calculation task 3 is identical with in task 4. In other words, under the situation of yielding, the new stress increments ($\dot{p}^{e}$, $\dot{q}^{e}$) calculated purely based on the elastic matrix need to be corrected into actual stresses increments ($\dot{p}$, $\dot{q}$) according to the plastic strain increments, elastic bulk modulus K and shear modulus G:

$$\dot{p} = \dot{p}^{e} - K\dot{\varepsilon}_{v}^{p} = K\dot{\varepsilon}_{v} - K\dot{\varepsilon}_{v}^{p} \qquad [11]$$

$$\dot{q} = \dot{q}^{e} - 3G\dot{\varepsilon}_{q}^{p} = 3G\dot{\varepsilon}_{q} - 3G\dot{\varepsilon}_{q}^{p} \qquad [12]$$

Based on the traditional plastic theory and normality where the plastic potential g (p,q,p_i) coincident with the yield surface f (p,q,p_i), the plastic flow during hardening is shown as:

$$\dot{\varepsilon}_{v}^{p} = \lambda_{h}\frac{\partial f}{\partial \sigma_{p}} \qquad [13]$$

$$\dot{\varepsilon}_{q}^{p} = \lambda_{h}\frac{\partial f}{\partial q} \qquad [14]$$

where λ_h is the scalar multiplier during hardening. The consistency condition for perfect plasticity is:

$$\dot{f} = \frac{\partial f}{\partial p}\dot{p} + \frac{\partial f}{\partial q}\dot{q} + \frac{\partial f}{\partial p_i}\dot{p}_i = 0 \quad [15]$$

By combining Eq. [3] and Eq. [11] - Eq. [14], the multiplier λ_h can be obtained. Assuming the stress dilatancy rule during unloading is perpendicular to that for loading, the stress dilatancy rule for unloading is then taken as negative of Eq. [2]. The plastic potential during unloading, following the conventional approach as Roscoe and Burland (1968) to derive the Cam Clay surface, can be obtained as:

$$g\left(p, q, p_i\right) = \ln\left(\frac{p}{p_i}\right) + \frac{1}{2}\ln\left|\frac{2\eta}{M_i}\right| - 1 \quad [16]$$

The consistency condition for perfect plasticity during unloading is:

$$\dot{g}\left(p, q, p_i\right) = \frac{\partial g}{\partial p}\dot{p} + \frac{\partial g}{\partial q}\dot{q} + \frac{\partial g}{\partial p_i}\dot{p}_i = 0 \quad [17]$$

It should be noticed that, during unloading the normality no longer apply as the plastic potential $g\ (p,q,p_i)$ is not coincident with the yield surface during unloading. Following the same procedure as deriving $\lambda_{h,,}$ the multiplier λ_s during softening can be obtained. The actual increments of stresses p and q considering plastic strains can then be recovered:

$$\dot{p} = K\dot{\varepsilon}_v - \lambda K\frac{\partial g}{\partial p} \quad [18]$$

$$\dot{q} = 3G\dot{\varepsilon}_q - 3\lambda G\frac{\partial g}{\partial q} \quad [19]$$

The implementation of Norsand is straightforward, the main effort is at calculation Task 2, where the plastic multiplier telling how far the plastic stresses go is calculated, and the state variables locating current yield

Norsand_subroutine
ID Task 1
Update state variables: locate current yield surfaces
ID Task 2
Apply strain increments $\dot{\boldsymbol{\varepsilon}}$ elastically to get new stress $\boldsymbol{\sigma}_e$
--- *Time integration*
Calculate M_i (COMI =1)

$$M_i = M\left(1 - \left|\psi_i\right| / M_{tc}\right)$$

Calculate f from:

$$f\left(p, q, p_i\right) = M_i\left[1 - \ln\left(\frac{p}{p_i}\right)\right] - \eta$$

If ($f \le 0$)
Then
End Norsand_subroutine (no plasticity)
Else
Stress correction

$$\dot{\varepsilon}^p_{v,q} = \lambda_h \frac{\partial f}{\partial \sigma_{p,q}}$$

$$\dot{\varepsilon}^p_{v,q} = \lambda_s \frac{\partial g}{\partial \sigma_{p,q}}$$

End If
--- *End time integration*
ID Task 3 OR 6
Define elastic matrix $\mathbf{D}_e$
ID Task 4
nStatv = 2 (number of state variables)
ID Task 5
Define Matrix type (stress dependent $\mathbf{D}_e$)
End Norsand_subroutine

Figure 4. Flow chart of Plaxis FORTRAN Norsand subroutine

surface are updated. The flow chart for the Norsand subroutine is shown in Figure 4. Details of compiling and coding the user defined subroutines in Plaxis can be found in Brinkgreve et al (2013).

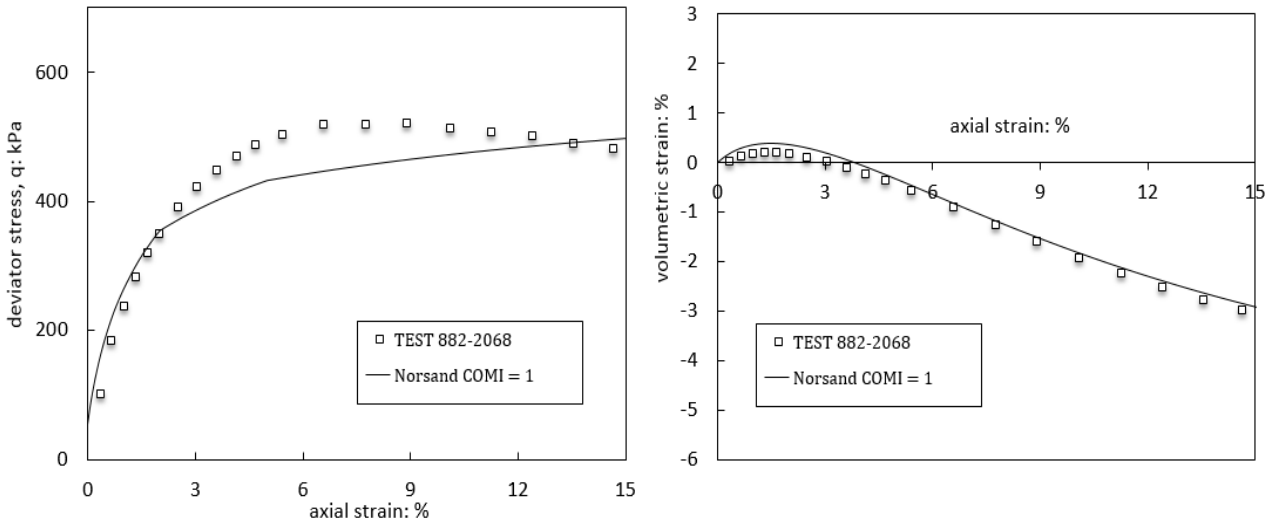

Figure 5. Numerical validation of Norsand with Leighton Buzzard sand (contraction negative)

The results

Leighton Buzzard Fraction E sand is used in the centrifuge tunnel (Marshall 2009), thus the same soil parameters will be adopted in the numerical modelling. Table 1 shows the soil parameters used in current research for Leighton buzzard sand. Each parameter holds clear physical meaning and can be identified though laboratory tests. Details of how to obtain the value of each parameter can be found in Jefferies and Shuttle (2005b).

Table 1. Parameters of Leighton buzzard sand

Γ	λ	M_{tc}	N	H_h	H_s	χ	I	ν	ψ
1.026	0.04	1.26	0.2	100	50	3.5	400	0.2	-0.115

a). Traxial compression test

For validation, the Norsand code is applied to simulate a traxial compression test using Leighton Buzzard sand performed by Golder Associate (test 882-2068). As shown in Table 1, the state parameter for the sand sample is -0.115 which implies a dense sand sample, thus should experience dilation followed by contraction during shearing. Modelling the dilation/ contraction behaviour, in other words, modelling volumetric strain increments, is the original intention of implementation of Norsand in Plaxis. In Figure 5, the laboratory test data is shown as square markers. COMI =1 (Jefferies and Shuttle, 2002) is found to give a better fit for this test and the numerical data is plotted in solid line. It can be seen that for the deviatoric stress q, there is a small deviation between the numerical and laboratory data (axial strain 3% ~ 12%). For the volumetric behaviour, the Norsand model gives a good fitting with the laboratory data.

b). The settlement troughs

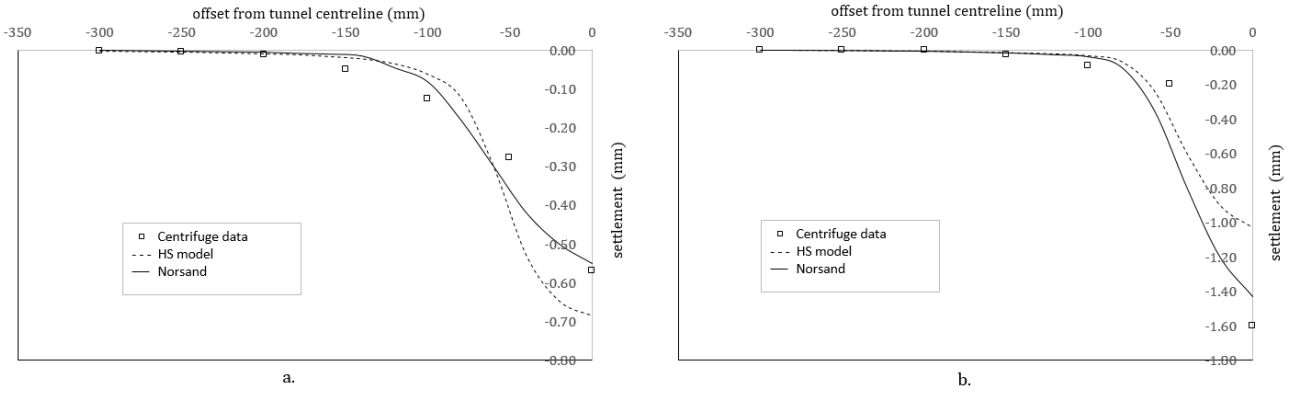

Figure 6. Settlement troughs at $V_{l,t}$ = 5 % a). 70mm deep b). 120mm deep

In the centrifuge test, the settlement data was recorded at depth of 0mm (surface), 70mm and 120mm with $V_{l,t}$ ranges from 0.5% to 5%. The settlement troughs at 70mm and 120mm deep with $V_{l,t}$ = 5% are plotted in Figure 6. The Hardening soil model (HS) over estimates the settlement trough at 70mm deep where the ground is experiencing dilation ($\dot{V}_{l,t}/\dot{V}_{l,s}$ ratio > 1) according to Marshall (2009). The contraction area (120mm deep where $\dot{V}_{l,t}/\dot{V}_{l,s}$ ratio <1) is under estimated by the HS model. In contrast, the Norsand model gives better prediction at both two depth levels.

Conclusions

In this work, the study interests are located on the contraction/ dilation behaviour of sand and its effect on the ground deformation induced by TBM tunnelling. These features of sand behaviour are well captured by the Norsand model, thus Norsand is implemented into a commercial geotechnical software-Plaxis 3D. The advantage of using the user defined model in Plaxis is that only the constitutive equations is needed in the subroutine, any other issues such as meshing and calculation algorithm are already well organised in the software.

In the traxial compression test, the Norsand code well predicted the volumetric strain development of a dense Leighton Buzzard sand sample. The efficiency of the Norsand model is proved in the more complicated green field tunnel model where the Norsand model gives reasonable settlement troughs in terms of shape and maximum settlement values. Localisation is not considered in the current Norsand subroutine, whereas shear bands are often observed in granular materials like sands (Rudnicki and Rice, 1975; Arslan and Sture, 2008). Future work could involve applying Norsand to more tunnel projects and introducing localisation into Norsand subroutine.

Acknowledgements

The authors would like to thank the “Geohazards risk assessment, mitigation and prevention” EU H2020 RISE programme for the financial support of this work.

References:

Arslan, H. and Sture, S. 2008. Finite element simulation of localization in granular materials by micropolar continuum approach. Computers and Geotechnics 35(4), pp. 548–562.

Azevedo, R. 2002. Numerical analysis of a tunnel in residual soils. Journal of Geotechnical and Geoenvironmental Engineering (March), pp. 227–236.

Been, K. and Jefferies, M. 1985. A state parameter for sands. Géotechnique 35(2), pp. 99–112.

Brinkgreve, R.B.. et al. 2013. PLAXIS Material Models Manual 2013. Delft: Plaxis bv.

Gonzalez, C. and Sagaseta, C. 2001. Patterns of soil deformations around tunnels. Application to the extension of Madrid Metro. Computers and Geotechnics 28, pp. 445–468.

Ishihara, K. et al. 1975. Undrained deformation and liquefaction of sand under cyclic stresses. Soils Fdns 15, pp. 29–44.

Jefferies, M. 1993. Nor-Sand: a simle critical state model for sand. Geotechnique 43(1), pp. 91–103.

Jefferies, M. and Been, K. 2006. Soil liquefaction. Abindon: Taylor & Francis.

Jefferies, M. and Shuttle, D. 2002. Dilatancy in general Cambridge-type models. Géotechnique 52(9), pp. 625–637.

Jefferies, M. and Shuttle, D. 2005a. NorSand: Features, calibration and use. In: Soil Constitutive Models. Austin, pp. 204–236.

Jefferies, M. and Shuttle, D. 2005b. Norsand:Features, Calibration and Use. In: Geo-Frontiers Congress 2005. Austin, Texas, United States: American Society of Civil Engineers.

Lee, C.J. et al. 2004. Ground movement and tunnel stability when tunneling in sandy ground. Journal of the Chinese Institute of Engineers 27(7), pp. 1021–1032.

Li, X. 1997. Modeling of dilative shear failure. Journal of Geotechnical and Geoenvironmental Engineering 123(July), pp. 609–616.

Li, X. et al. 1999. State-dependant dilatancy in critical-state constitutive modelling of sand. Canadian Geotechnical Journal 36, pp. 599–611.

Li, X. and Dafalias, Y. 2000. Dilatancy for cohesionless soils. Geotechnique 50(4), pp. 449–460.

Mair, R.J. et al. 1993. Subsurface settlement profiles above tunnels in clays. Geotechnique (2), pp. 315–320.

Mair, R.J. and Taylor, R.N. 1997. Theme lecture: Bored tunnelling in the urban environment. In: The 14th International Conference on Soil Mechanics and Foundation Engineering. pp. 2353–2385.

Manzari, M. and Dafalias, Y. 1997. A critical state two-surface plasticity model for sands. Geotechnique 47(2), pp. 255–272.

Marshall, A.M. 2009. Tunnelling in sand and its effect on pipelines and piles. University of Cambridge.

Marshall, A.M. et al. 2012. Tunnels in sands: the effect of size, depth and volume loss on greenfield displacements. Geotechnique (5), pp. 385–399.

Pinto, F. and Andrew J, W. 2000. Comparision of analytical solutions for ground movements caused by shallow tunnelling in soil. ASCE Journal of Engineering Mechanics.

Roscoe, K. and Burland, J. 1968. On the generalised stress-strain behaviour of 'wet' clay. In: Heyman, J. and Leckie FA eds. In Engineering Plasticity. Cambridge: Cambridge University Press, pp. 535–609.

Rowe, R.K. and Kack, G.J. 1983. A theoretical examination of the settlements induced by tunnelling: four case histories. Canadian Geotechnical Journal 20(2), pp. 299–314.

Rudnicki, J. and Rice, J. 1975. Conditions for the localization of deformation in pressure-sensitive dilatant materials. Journal of the Mechanics and Physics of Solids 23(1970), pp. 371–394.

Schanz, T. et al. 1999. The hardening soil model: formulation and verification. Beyond 2000 in computaional Geotechnics, pp. 1–16.

Schofield, A. and Wroth, P. 1968. Critical state soil mechanics. London: McGrawHill.

Vorster, T.E.B. et al. 2005. Estimating the effects of tunneling on existing pipelines. Journal of Geotechnical and Geoenvironmental Engineering (November), pp. 1399–1410.